JMEPEG (2012) 21:1416–1421
DOI: 10.1007/s11665-011-0009-y

1059-9495/$19.00

Mechanical Properties of INCONEL 718 Parts Manufactured by Shaped Metal Deposition (SMD)

Bernd Baufeld

(Submitted December 9, 2010; in revised form July 7, 2011)

INCONEL 718 parts have been manufactured by shaped metal deposition (SMD), an additive layer manufacturing technique applying wire-based tungsten inert gas welding. This technique is aimed toward mass customization of parts, omitting time- and scrap-intensive, subtractive fabrication routes. SMD results in dense, "near net-shaped" parts without pores, cracks, or fissures. The microstructure of the SMD parts exhibit large, columnar grains with a fine dendritic microstructure. The interdendritic boundaries are decorated by small Laves phase precipitates and by MC carbides. Tensile tests were performed with different strain rates (10^{-4}, 10^{-3}, and 2×10^{-3} 1/s), but no dependency on strength or strain at failure was observed. The ultimate tensile strength was 828 ± 8 MPa, the true plastic strain at failure 28 ± 2%, the micro Vickers hardness 266 ± 21 HV200, and the dynamically measured Young's module was 154 ± 1 GPa.

Keywords additive manufacturing, aerospace, electron microscopy, fabricated metal, mechanical testing, shaped metal deposition, welding

1. Introduction

Additive manufacturing is a novel concept, where near net-shaped parts are created layer wise. In comparison with traditional subtractive methods, scrap material and machining times are largely reduced. Additive manufacturing allows accelerating the introduction of new designs, shortening the product implementation cycle, and being applied for the repair of expensive components. While additive manufacturing is not suitable for mass production, it is ideal for mass customization (Ref 1). Different methods, each with their characteristic pro and cons, are under investigation applying different heat sources, such as laser beam, electron beam, or welding torch, and supplying the material either in form of powder or wire. The method applied for the present article is called shaped metal deposition (SMD), which is utilizing a tungsten inert gas (TIG) welding torch and is fed by wire.

Until now SMD has been used mostly to build Ti-6Al-4V parts (Ref 2-9), which is the most widely applied Ti alloy (Ref 10). Ti alloys are expensive and difficult to machine, which makes additive manufacturing a perfectly fitting technique. SMD was also applied for Ti and intermetallics (Ref 11), different steels (Ref 12, 13), and INCONEL 718 (Ref 14). The latter is today's superalloy of choice for a wide variety of turbine engine applications, making up 55-70% of the nickel base superalloys in modern jet engines (Ref 15). The emphasis of the present article is on the material properties of SMD parts of this alloy, which has not been studied by Clark et al. (Ref 14). While here the properties of as-fabricated parts are investigated, a future article will show the influence of heat treatment (Ref 16).

Detailed knowledge of the microstructure and the properties is the prerequisite to achieve reliability and consistency of an additive manufacturing technique, which is necessary for a successful transition from the experimental state to manufacturing (Ref 17). It was predicted, but not proven by Clark et al., that SMD has the inherent potential to outperform polycrystalline castings of the same chemistry in terms of mechanical properties, because of the more consistent solidification conditions made possible by a deposition process (Ref 14). The microstructure and mechanical properties for INCONEL 718 parts fabricated by other additive manufacture techniques, such as electron (Ref 18, 19) or laser beam (Ref 20-22), have already been investigated, and the results will be compared in this study.

2. Experimental

2.1 SMD Unit

The SMD unit consists of a 6-axis KUKA KR16 robot manipulating a Fronius Tungsten Inert Gas (TIG) welding head and a 2-axis DKP400 turntable, all located in an airtight chamber filled with argon of 99.999% purity. The INCONEL 718 wire of 1.2-mm diameter is supplied by a Fronius wire feeder located outside of the chamber. The material was deposited by single track, layer by layer with a step height of 1 mm on an INCONEL 718 plate. The geometry of the targeted part was a square-based tube with 0.17-m side length, 0.12-m height, and 0.01-m wall thickness (Fig. 1). The applied SMD parameters were a wire feed speed of 1.5 m/min, a deposition speed of 0.3 m/min, and an electrical current of 220 A. These parameters lead to fully dense parts without pores, cracks, or fissures.

Bernd Baufeld, Nuclear Advanced Manufacturing Research Centre, University of Sheffield, Brunel Way, Rotherham S60 5WG, UK. Contact e-mail: b.baufeld@sheffield.ac.uk.

The coordinate system applied in the present article attributes x to the travel direction of the TIG head relative to the base plate, y to the direction perpendicular to the wall surface, and z to the direction perpendicular to base plate.

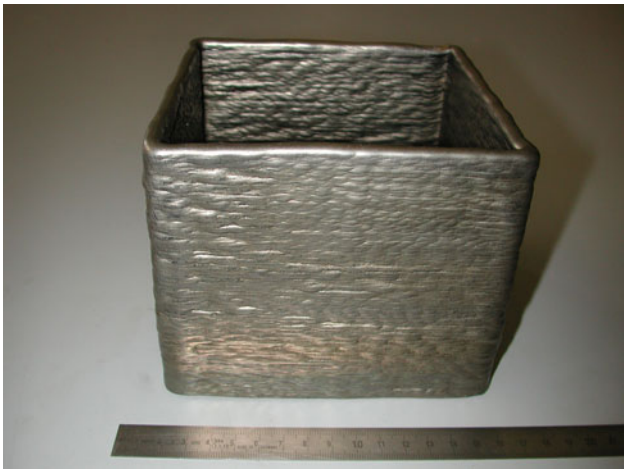

Fig. 1 View on a square-based, tubular INCONEL 718 part

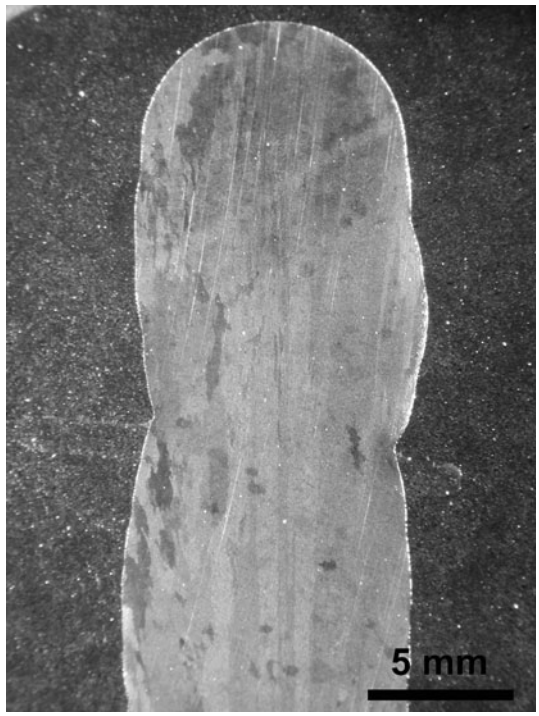

Fig. 2 Top area of part in y-z cross section

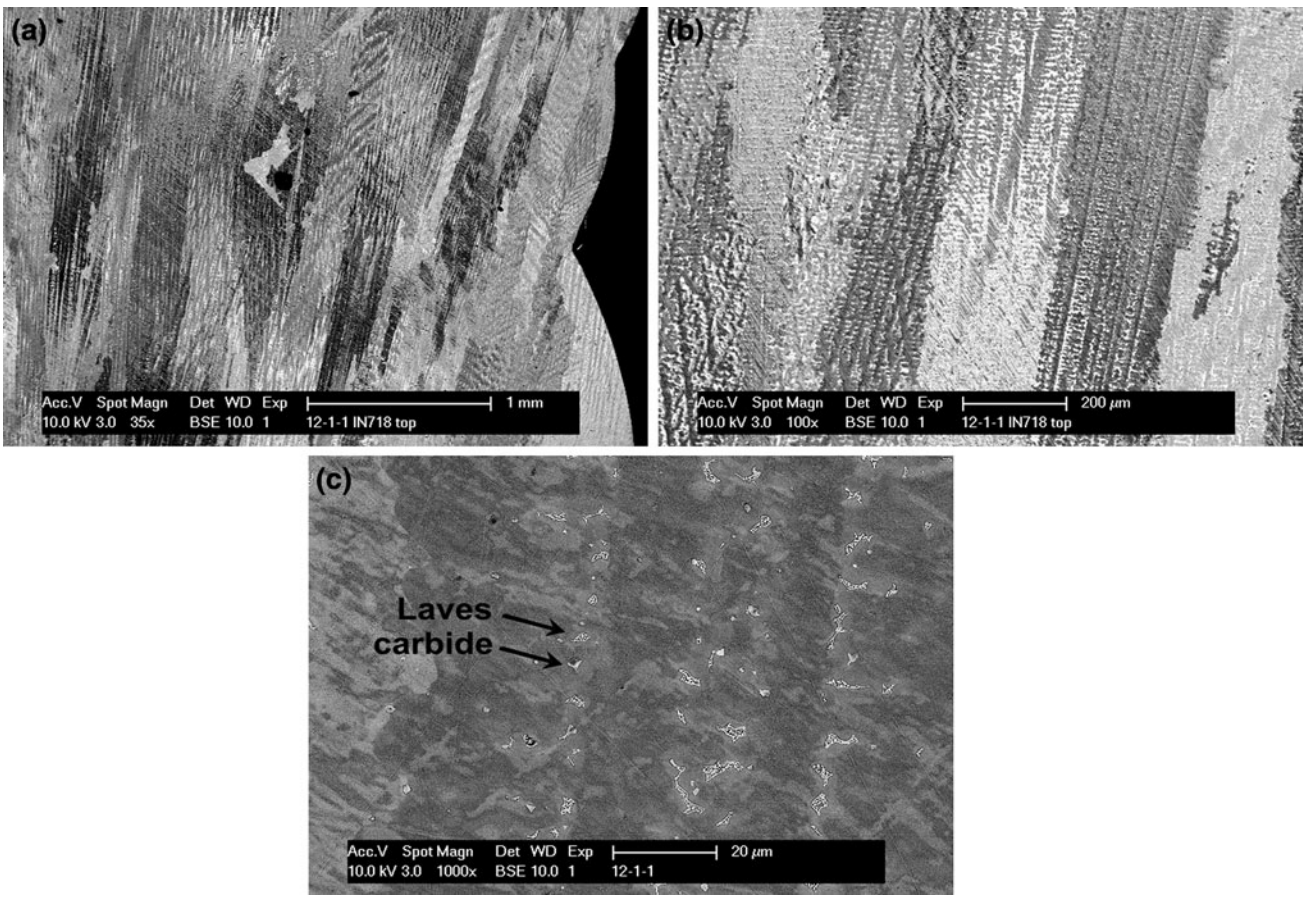

Fig. 3 SEM micrographs (y-z plane) exhibiting the elongated grains and the dendritic microstructure at different magnifications (a–c). (a) Contour of the wall surface at right

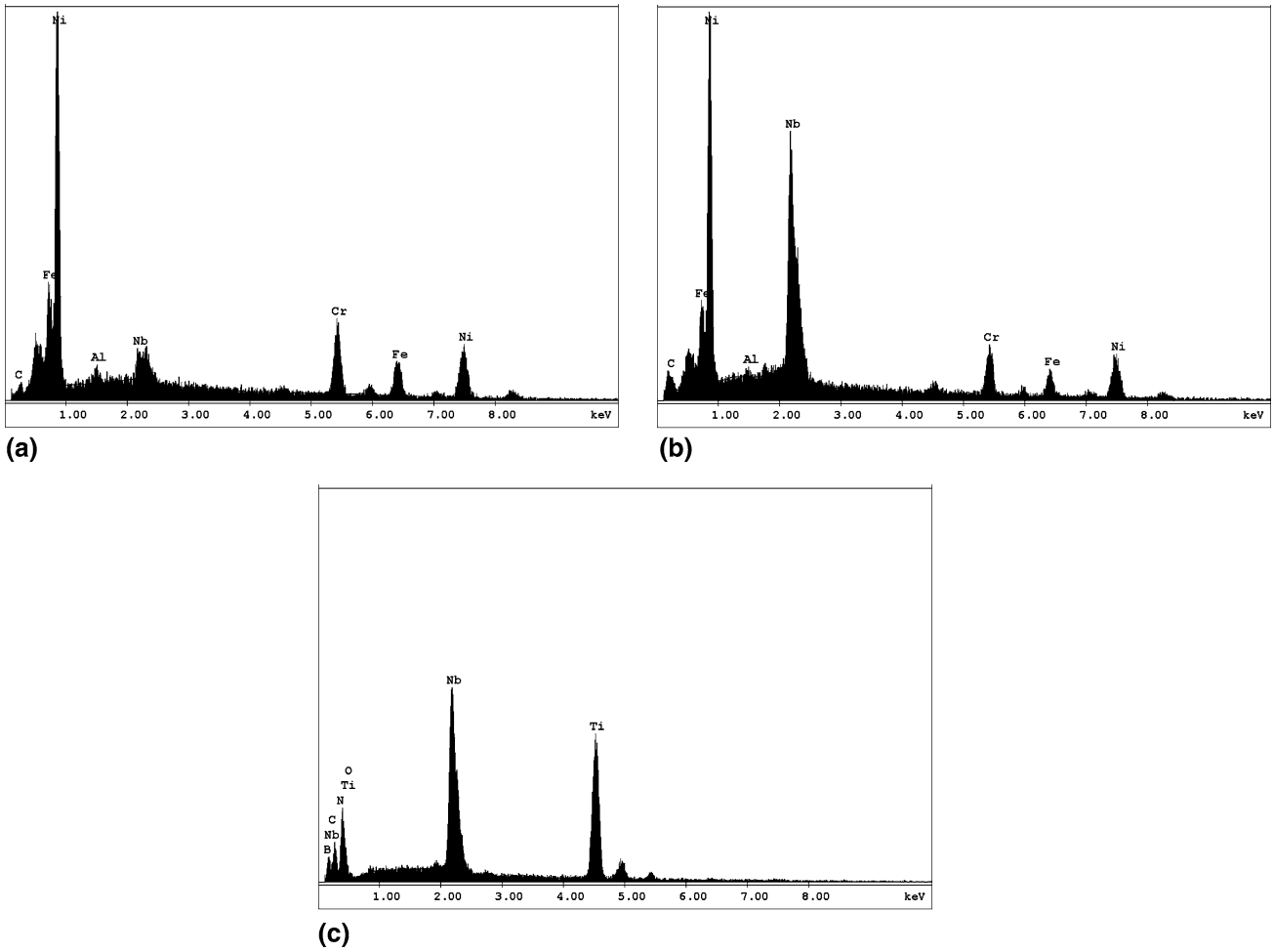

Fig. 4 EDX spectra from matrix (a), Laves phase (b), and MC-type carbide (c)

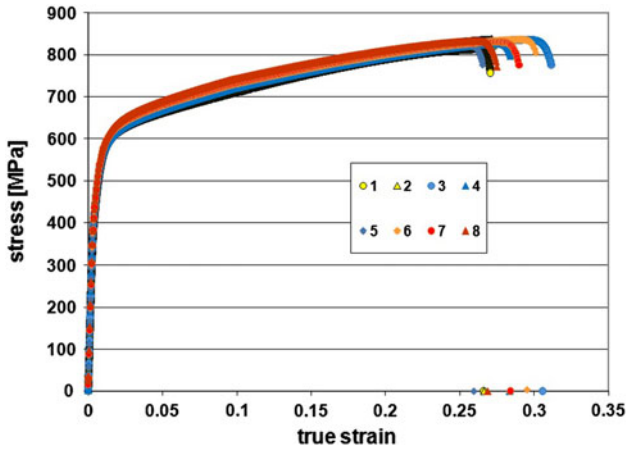

Fig. 5 Stress-true strain curves of INCONEL 718 SMD specimens tested with different strain rates: 10^{-4} 1/s (1, 2), 10^{-3} 1/s (3, 4, 5), and 2×10^{-3} 1/s (6, 7, 8)

2.2 Mechanical Testing and Microstructure Characterisation

The tensile testing was performed with an Instron testing machine model 4505 under strain rate control, applying an extensometer with a gauge length of 25 mm, and different strain rates, namely, 10^{-4} 1/s (specimen 1 and 2), 10^{-3} 1/s (specimen 3, 4, and 5), and 2×10^{-3} 1/s (specimen 6, 7, and 8). The strain at failure was determined from the plastic true strain at failure. Flat dog bone-shaped tensile specimens with a 4×2 mm^2 cross section were cut by electrical discharge machining, with their tensile axis perpendicular to the deposition plane, and then grinded. The Young's modulus was not only derived from the elastic part of the stress-strain curve, but also by applying the impulse excitation technique (Ref 23) (IMCE, Diepenbeek, Belgium). The specimen was a bar with the dimensions of $25 \times 8 \times 3$ mm^3.

Optical and scanning electron microscopy (SEM, FEI XL30FEG) on polished or etched (with NITAL) cross sections was applied to investigate the microstructure. Energy dispersive x-ray spectrometry was applied for elemental analysis.

The Vickers microhardness was measured with a Leitz microhardness tester with a load of 200 g. Several indents on a *y-z* plane at different heights relative to the base plane were executed.

3. Results

3.1 Shape, Morphology, and Microstructure

The surface of the INCONEL 718 SMD walls is rippled reflecting the layerwise deposition. The top side is round due to

the surface tension in the liquid state (Fig. 1). The optical micrograph of the etched cross section exhibits large, columnar grains extending in the direction of the wall height across many deposition layers (Fig. 2). No pores, cracks, or regions of bad fusion are observed.

The SEM of Fig. 3(a) shows in more detail these grains in addition to the contour of the rippled surface. The ripples derive from the melt of subsequent SMD steps, and it is worthy to note that no interrelation between the grains and the ripples is observable. In contrast to reports from additive manufacturing of INCONEL 718 applying laser (Ref 21) or electron beam techniques (Ref 18), no evidence of banded structures reflecting the individual passes of the deposition is found.

The grains consist of a fine dendritic microstructure with different precipitates, characterizing the interdendritic boundaries (Fig. 3b, c). After etching the cross section, one type of precipitates shows a substructure, while the other does not. Examples of EDX spectra from the matrix and from the two different types are given in Fig. 4. Compared to the matrix (Fig. 4a), the precipitates with substructure is rich in Nb (Fig. 4b), while the other type contains Nb, Ti, and lighter elements, such as C, N, and B (Fig. 4c). According to the literature, the microstructure of Inconel 718 is governed by the fcc lattice structure of the γ matrix and a number of characteristic precipitates, where not only the chemical compositions of the precipitates but also by their distribution, location, and possible coagulation during thermal and mechanical treatments are decisive in the microstructural development (Ref 24). In weld metals and heat-affected zones, the two main

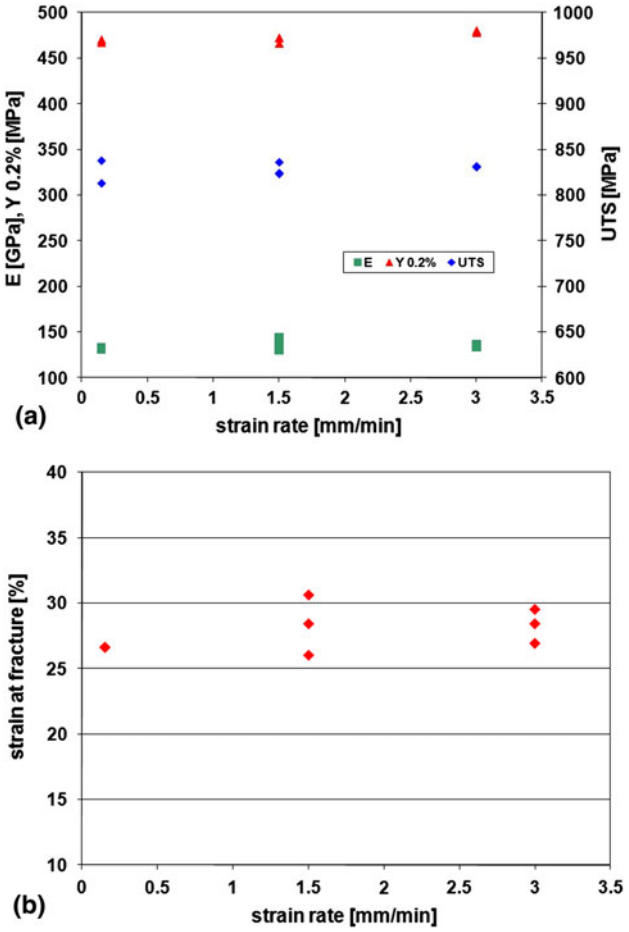

Fig. 6 Compilation of test results depending on the strain rate. (a) Ultimate tensile strength (UTS), yield strength at 0.2% $\sigma_{0.2\%}$, and Young's modulus *E*. (b) Plastic true strain at failure

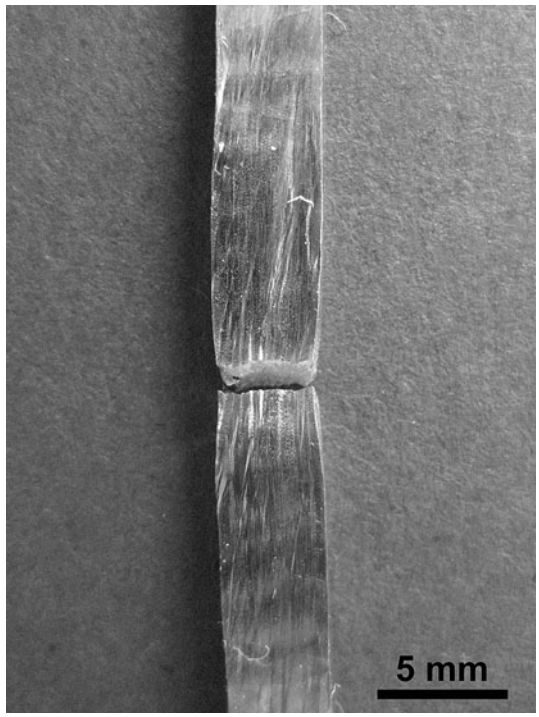

Fig. 7 Tensile specimen after failure

Table 1 Mechanical properties of SMD parts in comparison of additive manufactured by laser or electron beam and of as-cast material

	UTS, MPa	$\sigma_{0.2\%}$, MPa	*E*, GPa	$\varepsilon_{plastic}$, %
SMD	828 ± 8	473 ± 6	Stress-true strain: 135 ± 4 IET: 154 ± 1	28 ± 2
Laser (Ref 19)	845	590	n.a.	11
Laser (Ref 20)	1000	650	n.a.	n.a.
Laser (Ref 21)	904	552	n.a.	16
Electron beam (Ref 18)	910	580	159	22
As cast (Ref 18)	786	488	n.a.	22

n.a.: not analyzed

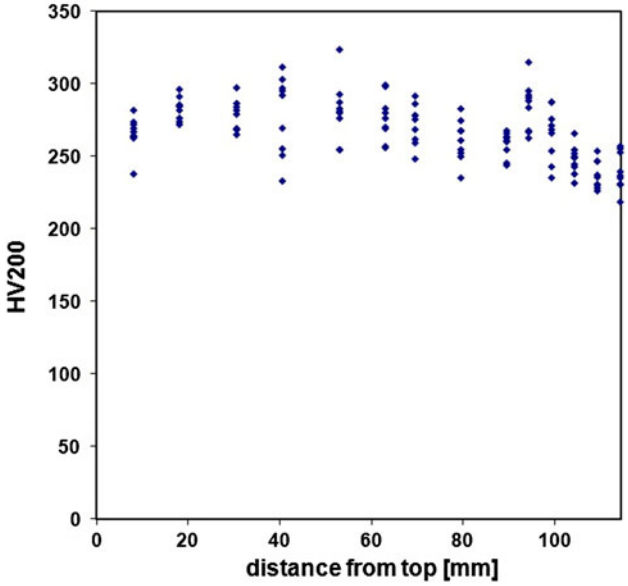

Fig. 8 Micro Vickers hardness in dependence on the distance from the top (*y*-*z* plane)

types of precipitates are Nb-rich Laves phase and Nb(Ti)-rich MC-type carbides (Ref 25). Accordingly, the precipitates with substructure have been attributed to the Laves phase, and the other to the MC carbides (Fig. 3).

3.2 Mechanical Testing

Figure 5 presents the stress-true strain curves for different strain rates. All the curves exhibit yielding, extensive plasticity with strain hardening, and comparable values of strength and strain at failure. As the compilation of the results shows (Fig. 6), no strain rate sensitivity is observed. In Table 1, the averages, from all the eight experiments, of the ultimate tensile strength, UTS, the yield strength $\sigma_{0.2\%}$, the Young's modulus E, and the plastic true strain $\varepsilon_{plastic}$ as an indication for the ductility are compared with results of parts additive manufactured by laser and electron beam, and, in addition, with the properties of as-cast material. The strength and strain values of SMD specimens are comparable or slightly better than as reported for the as-cast material. Compared with specimens from additive manufactured by laser or electron beam, their strengths are inferior, and their plastic strain at failure values are superior. Naturally the strength of the as-deposited material is lesser in comparison to that of wrought material or to that of material subjected to special heat treatment for performance improvement, and dedicated heat-treatment promises improvements (Ref 20-22). However, improved strength may be accompanied with decreased ductility (Ref 20-22). This will be investigated in a future article (Ref 16).

The Young's modulus, derived from the stress-true strain curve, is 135 GPa. However, the determination of the Young's modulus by this method may include some experimental error (IET); a much more reliable method, gives 154 GPa. This value agrees very well with results reported for INCONEL 718 parts additive manufactured by electron beam (Ref 18). Nevertheless, these results are much lower than the Young's modulus of 206 MPa reported by Fukuhara for INCONEL 718 (Ref 26). The authors of Ref 18 have attributed the low values to the strong texture of additive manufactured parts.

Figure 7 shows a specimen after failure exhibiting a distinctive surface relief and necking due to the extensive plasticity before the final fracture. Noteworthy is the development of a banded structure parallel to the deposition plane of the SMD component, possibly reflecting the deposition layers.

Figure 8 shows the micro Vickers hardness depending on the distance from the top. As usually observed for microhardness measurements, the results exhibit a large scatter. Within this scatter, no clear dependency of the results on the location can be reported. If at all, the values are slightly lower near the base plate. The average of all the results gives 266 ± 21 HV200.

4. Conclusions

It has been shown that the additive layer manufacturing method of SMD is suitable for near net-shaped processing of dense INCONEL 718 parts, introducing this technique for mass customization. The tensile strengths of these parts are slightly higher than that of the as-cast material but lower than those of parts fabricated by other additive layer manufacturing techniques. This is possibly related to the lower cooling rates than in the case of techniques based on laser or electron beam. The true strain at failure of SMD specimens proved to be superior to specimens from parts fabricated by other additive layer manufacturing techniques or from the as-cast material. Dedicated heat treatment possibly can increase the strength of SMD parts, but probably at the expense of the ductility. The choice of this technique will therefore depend on the application according as whether a higher strength or ductility is preferred.

Acknowledgments

The research has been performed as part of the RAPOLAC STREP project under contract number 030953 of the Sixth Framework Programme of the European Commission (http://www.RAPOLAC.eu), which is gratefully acknowledged. The parts have been built at AMRC, Sheffield, the United Kingdom in association with the team of Dr. Rosemary Gault, and the experimental evaluation has been performed at the Katholieke Universiteit Leuven, Belgium, in association with tthe team of Prof. Omer van der Biest. The supports provided by them and their staff are highly acknowledged.

References

1. K. Cooper and S. Lambrakos, Thermal Modeling of Direct Digital Melt-Deposition Processes, *J. Mater. Eng. Perform.*, 2011, **20**, p 48–56
2. C. Charles and N. Järvstrat, Development of a Microstructure Model for Metal Deposition of Titanium Alloy Ti-6Al-4V, *11th World Conference on Titanium (Ti-2007)* (Kyoto, Japan), 2007, p 1201–1204
3. C. Charles and N. Järvstrat, Modelling Ti-6Al-4V Microstructure by Evolution Laws Implemented as Finite Element Subroutines: Application to TIG Metal Deposition, *8th International Conference on Trends in Welding Research*, (Pine Mountain, GA), 2008
4. B. Baufeld and O. van der Biest, Mechanical Properties of Ti-6Al-4V Specimens Produced by Shaped Metal Deposition, *Sci. Technol. Adv. Mater.*, 2009, **10**, p 10
5. B. Baufeld, O. van der Biest, and S. Dillien, Texture and Crystal Orientation in Ti-6Al-4V Builds Fabricated by Shaped Metal Deposition, *Met. Mater. Trans. A*, 2009, **41**, p 1917–2010

6. B. Baufeld, O. van der Biest, and R. Gault, Microstructure of Ti-6Al-4V Specimens Produced by Shaped Metal Deposition, *Int. J. Mater. Res.*, 2009, **100**, p 1536–1542
7. B. Baufeld, O. van der Biest, and R. Gault, Additive Manufacturing of Ti-6Al-4V Components by Shaped Metal Deposition: Microstructure and Mechanical Properties, *Mater. Des.*, 2010, **31**, p S106–S111
8. B. Baufeld, O. van der Biest, R. Gault, and K. Ridgway, Manufacturing Ti-6Al-4V Components by Shaped Metal Deposition: Microstructure and Mechanical Properties, *TRAM 2009, IOP Conference Series: Materials Science and Engineering* (Sheffield, UK), 2010
9. A.K. Swarnakar, O. van der Biest, and B. Baufeld, Thermal Expansion and Lattice Parameters of Shaped Metal Deposited Ti-6Al-4V, *J. Alloy Compd.*, 2011, **509**, p 2723–2728
10. C. Leyens and M. Peters, *Titanium and Titanium Alloys*, Wiley-VCH, Weinheim, 2003
11. M. Katou, J. Oh, Y. Miyamoto, K. Matsuura, and M. Kudoh, Freeform Fabrication of Titanium Metal and Intermetallic Alloys by Three-Dimensional Micro Welding, *Mater. Des.*, 2007, **28**, p 2093–2098
12. T. Skiba, B. Baufeld, and O. van der Biest, Microstructure and Mechanical Properties of Stainless Steel Component Manufactured by Shaped Metal Deposition, *ISIJ Int.*, 2009, **49**, p 1588–1591
13. T. Skiba, B. Baufeld, and O. van der Biest, Shaped Metal Deposition of 300M Steel, *Proc. IME B J. Eng. Manufact.*, 2011, **255**, p 831–839
14. D. Clark, M. Bache, and M. Whittaker, Shaped Metal Deposition of a Nickel Alloy for Aero Engine Applications, *J. Mater. Process. Technol.*, 2008, **203**, p 439–448
15. R.A.J. Jeniski and R.L. Kennedy, Nickel-base Superalloy Designed for Aerospace, *Adv. Mater. Process.*, 2006, **164**, p 19–22
16. B. Baufeld and A.K. Swarnakar, Influence of Heat Treatment on the Mechanical Properties of IN718 Parts Built by Shaped Metal Deposition (SMD), in preparation
17. S.G. Lambrakos and K.P. Cooper, An Algorithm for Inverse Modeling of Layer-by-Layer Deposition Processes, *J. Mater. Eng. Perform.*, 2009, **18**, p 221–230
18. R.K. Bird and J. Hibberd, Tensile Properties and Microstructure of INCONEL 718 Fabricated with Electron Beam Freeform Fabrication (EBF3), *NASA* (Hampton, VA), 2009, p 14
19. J.E. Matz and T.W. Eagar, Carbide Formation in Alloy 718 During Electron-Beam Solid Freeform Fabrication, *Metall. Mater. Trans. A*, 2002, **33**, p 2559–2567
20. X. Zhao, J. Chen, X. Lin, and W. Huang, Study on Microstructure and Mechanical Properties of Laser Rapid Forming INCONEL 718, *Mater. Sci. Eng. A*, 2008, **478**, p 119–124
21. P.L. Blackwell, The Mechanical and Microstructural Characteristics of Laser-Deposited IN718, *J. Mater. Process. Technol.*, 2005, **170**, p 240–246
22. H. Qi, M. Azer, and A. Ritter, Studies of Standard Heat Treatment Effects on Microstructure and Mechanical Properties of Laser Net Shape Manufactured INCONEL 718, *Metall. Mater. Trans. A*, 2009, **40**, p 2410–2422
23. G. Roebben, B. Bollen, A. Brebels, J. van Humbeeck, and O. van der Biest, Impulse Excitation Apparatus to Measure Resonant Frequencies, Elastic Moduli, and Internal Friction at Room and High Temperature, *Rev. Sci. Instrum.*, 1997, **68**, p 4511–4515
24. A.J. Brand, K. Karhausen, and R. Kopp, Microstructural Simulation of Nickel Base Alloy INCONEL 718 in Production of Turbine Discs, *Mater. Sci. Technol.*, 1996, **12**, p 963–969
25. G. Knorovsky, M. Cieslak, T. Headley, A. Romig, and W. Hammetter, INCONEL 718: A Solidification Diagram, *Metall. Mater. Trans. A*, 1989, **20**, p 2149–2158
26. M. Fukuhara and A. Sanpei, Elastic Moduli and Internal Frictions of INCONEL 718 and Ti-6Al-4V as a Function of Temperature, *J. Mater. Sci. Lett.*, 1993, **12**, p 1122–1124